JOURNAL OF SPACECRAFT AND ROCKETS
Vol. 45, No. 3, May–June 2008

Autonomous Orbit Determination from Lunar Halo Orbits Using Crosslink Range

Keric Hill* and George H. Born†
University of Colorado, Boulder, Colorado 80309

DOI: 10.2514/1.32316

Liaison navigation is a method of autonomous, interplanetary orbit determination where scalar satellite-to-satellite measurements, such as crosslink range, are used to estimate the orbits of all participating spacecraft simultaneously. Crosslink range can be used to observe the orbit states for all participating spacecraft in the circular, restricted, three-body problem, as long as one of the spacecraft is in an orbit at L_1 or L_2. In the two-body problem, only the relative orbits can be estimated using crosslinks, but when three-body dynamics dominate, it enables the estimation of both relative and absolute orbit states. To add realism in this study, navigation simulations were performed again, but this time the spacecraft trajectories were propagated in an inertial frame using the DE403 ephemeris for the planets. Also, a 50th degree and order lunar spherical harmonic gravity field, solar radiation pressure, and maneuvers were simulated, with appropriate modeling errors. Four different lunar constellations were analyzed with applications to lunar navigation and communication relay. An extended Kalman filter was used to process the measurements. The results show that real-time, on-board position accuracies on the order of 100 m root sum square are possible for lunar libration point orbiters, and solutions on the order of 10 m root sum square are possible for lunar orbiters.

Nomenclature

$\mathbf{c}_{\text{clone}}$	=	clone of the vector $\mathbf{c}_{\text{grav}}$
$\mathbf{c}_{\text{grav}}$	=	vector of normalized coefficients in a spherical harmonic gravity model
$\mathbf{e}$	=	vector of normally distributed random numbers with zero mean and unit variance
P_{grav}	=	covariance matrix representing the errors in $\mathbf{c}_{\text{grav}}$
P_k	=	estimation error covariance matrix at time t_k, computed after the measurement update
$\bar{P}_k$	=	estimation error covariance matrix at time t_k, computed before the measurement update
Q	=	state noise compensation portion of the time update equation in the extended Kalman filter
S	=	upper triangular factorization of P_{grav}
Δt	=	time interval between observations
θ	=	inclination of the lunar equator with respect to the Earth's mean equator
σ_i^2	=	variance for an unknown acceleration
$\Phi(t, t_k)$	=	state transition matrix mapping state deviations from time t_k to time t
ϕ	=	rotation from the equinox to the ascending node of the lunar equator
ψ	=	angle along the lunar equator from the node to a longitude of zero

I. Introduction

THE most common procedure for estimating the orbit of an interplanetary spacecraft is to use tracking stations on the Earth to obtain radiometric measurements [1]. Measurements between spacecraft can be used to reduce the dependence on Earth-based observations and reduce operations costs. Scalar radiometric tracking measurements taken along the line of sight between the two spacecraft, such as range or Doppler, would be a relatively easy way of obtaining tracking data, but these do not usually provide information on the absolute orientation of the orbits. Thus, when using only scalar satellite-to-satellite tracking (SST) data, the state or ephemeris of one of the spacecraft would usually have to be fixed for the absolute orientation of the orbits to be observable.

According to an analysis by Markley [2], a state is unobservable if a deviation in the state can be found that does not result in any change in the observations. Because changes in the size, shape, or relative orientation of two orbits will affect scalar SST measurements, scalar SST between two spacecraft can be used to observe those parameters, except in a few specific situations. It has been shown that the nature of the two-body problem is the reason for the unobservability of the absolute orientation when using only scalar SST [3]. In the two-body problem, both spacecraft orbits can be rotated around the center of mass of the central body. If both are given the same rotation, due to the symmetry in the two-body problem, the orbits will have the same size, shape, and relative orientation and the measurements will not be affected. Effectively, scalar radiometric measurements cannot observe the change in absolute orientation in this case. To observe the relative and absolute orbit states of both spacecraft simultaneously in the two-body problem, Markley and Psiaki [4] showed that inertially referenced intersatellite angles obtained with something like an optical imager would have to be used in addition to scalar SST data.

In the three-body problem, the gravitational influence of the third body influences the dynamics of a spacecraft and can provide information about the orientation of the spacecraft orbit with respect to both the third body and the central body. If the absolute states of the planetary bodies are known, then the absolute states of all the spacecraft can be estimated simultaneously using only scalar SST. A new method of autonomous orbit determination called "liaison navigation" was recently presented in which spacecraft use scalar SST data, such as crosslink range, to determine the orbits of all participating spacecraft [3]. In certain orbits, liaison navigation can be used to estimate both the absolute and relative states of all the participating spacecraft simultaneously, without any mathematical constraints. Simulations showed that the crosslink range could be used to estimate the states of two spacecraft simultaneously in the circular, restricted, three-body problem (CRTBP), when at least one of the spacecraft was in a region in which three-body dynamics dominate the orbital motion. The vicinities of either the Lagrange point L_1 or L_2 satisfy this requirement. Those simulations included

Received 25 May 2007; revision received 28 September 2007; accepted for publication 28 September 2007.

*Graduate Research Assistant, Colorado Center for Astrodynamics Research, Campus Box 429. Member AIAA.

†Director, Colorado Center for Astrodynamics Research, Campus Box 431. Fellow AIAA.

only data noise, with no modeling errors. To add more realism in this study, realistic force models and modeling errors were used for orbit propagation and determination, instead of using the simplified dynamics of the CRTBP. The resulting high-fidelity simulations show that liaison navigation works very well for several useful lunar constellations in a realistic modeling environment.

II. Realistic Orbit Dynamics

"Truth" orbits were propagated and used to generate crosslink measurements and for filter accuracy comparisons. However, when integrating the orbits in the orbit determination filter, some modeling errors were introduced to add realism.

Both the truth orbits and the orbits with modeling errors were generated using the TurboProp software package [5]. The planetary ephemeris DE403 from NASA's Jet Propulsion Laboratory [6] was used to compute the positions and the point-mass gravitational influence of the Earth, moon, sun, Venus, Mars, Jupiter, and Saturn. This ephemeris provides planetary positions in the international celestial reference frame (ICRF) [7]. The ephemeris files are in ASCII format, but they can be converted into binary and the resulting file can then be efficiently queried to provide planetary positions and velocities at the desired epoch. This was done by modifying C code written by Hoffman [8].

For propagating the orbits of lunar orbiters and halo orbiters, LP100K was used as a precise model of the moon's gravity field [9]. For Earth orbiters, JGM-3 was used as the Earth's gravity model [10]. These models were truncated after degree and order 50. To simulate gravity modeling errors, a clone of the lunar gravity field was created by randomly perturbing the gravity field coefficients using the covariance matrix for the LP100K model. The vector $\mathbf{c}_{\text{grav}}$ includes all of the normalized coefficients in the gravity model and the corresponding covariance matrix is P_{grav}. A clone of the gravity model can be created by factoring P_{grav}:

$$P_{\text{grav}} = S^T S \tag{1}$$

S is the upper triangular and can be computed using Cholesky cecomposition. If $\mathbf{e}$ is a vector of normally distributed random numbers with zero mean and unit variance, a clone of the gravity model, $\mathbf{c}_{\text{clone}}$ would be

$$\mathbf{c}_{\text{clone}} = \mathbf{c}_{\text{grav}} + S^T \mathbf{e} \tag{2}$$

The orientation of the Moon was computed using the lunar librations from the DE403 ephemeris. These are three Euler angles, which are ϕ, the rotation angle along the Earth's mean equator of J2000 from the equinox to the ascending node of the lunar equator, θ, the inclination of the lunar equator with respect to the Earth's mean equator, and ψ, the angle along the lunar equator from the node to a longitude of zero [11].

The conversion from the Earth-centered inertial frame based on the ICRF, or the geocentric celestial reference frame (GCRF), to the Earth-fixed frame was computed using the 1976 International Astronomical Union (IAU) precession, 1980 IAU nutation [with International Earth Rotation and Reference Systems Service (IERS) corrections and offsets for GCRF], Earth rotation, and polar motion [12].

Solar radiation pressure (SRP) was modeled using an umbra/penumbra eclipse model. The solar pressure was computed based on the spacecraft's distance from the sun, with a flux of 1358 W/m^2 at 1 astronomical unit (AU). All satellites were modeled as 1000-kg spheres with a cross-sectional area of 5 m^2. To simulate radiation modeling errors, the reflectance parameters of the spacecraft were randomly perturbed so that acceleration errors were on the order of 10^{-9} m/s^2, a typical value for interplanetary spacecraft. The perturbed reflectance parameters were fixed in the estimation process so they would not be adjusted by the filter.

In most of the simulations, one spacecraft was in a halo orbit at either L_1 or L_2 in the Earth-moon system. Halo orbits were first named by Farquhar [13] and are periodic orbits in the CRTBP. For this study, lunar halo orbits were computed initially in the CRTBP using the technique explained by Howell [14], and then converted to the ephemeris model of the solar system. In the ephemeris model, there are no longer any periodic solutions, meaning that the periodic halo orbits found in the three-body problem do not occur. Instead, a halo orbit from the CRTBP is first rotated and scaled to fit the inertial frame, usually a moon-centered frame based on the ICRF. Then the trajectory is differentially corrected until one is found that is continuous and fairly close to periodic. The resulting quasi-periodic orbits are near the original halo orbits and are functionally the same. The numerical method used to find these halo orbits in the ephemeris model was a multiple shooting differential corrector adapted from the work of Howell and Pernicka [15].

For the halo orbits, nominal trajectories were generated using the multiple shooting differential corrector and divided into four segments per halo orbit period. These segments were usually about 3.5 days in length. Because of navigation errors coupled with the unstable dynamics of a halo orbit, the halo orbiter is never exactly on the desired nominal orbit at the segment end time, so a stationkeeping maneuver (SKM) must be performed to bring the halo orbiter closer to the nominal orbit. This was done with the same method used for the Genesis Mission [16], in which the spacecraft velocity is differentially corrected to target the position and time at the end of the next segment of the nominal orbit. In this case, a simulated on-board estimate of the state is used to initialize the SKM targeter instead of the truth orbit. The difference between the current velocity and the corrected velocity is applied as an impulsive ΔV, but random, normally distributed thruster errors with a standard deviation of 5% were added for each component of the ΔV.

III. Orbit Determination

A real-time state update provides spacecraft with accurate orbit determination quickly, allowing spacecraft to be used as navigation support for other missions and reducing dependence on Earth-based operations. An extended Kalman filter (EKF) is relatively simple and provides real-time state estimates, so it was ideal for this purpose. A description of how to implement the EKF can be found in Tapley et al. [17]. To prevent filter saturation, state noise compensation was performed by adding a matrix Q to the time update of the estimation error covariance matrix:

$$\bar{P}_k = \Phi(t_k, t_{k-1}) P_{k-1} \Phi^T(t_k, t_{k-1}) + Q \tag{3}$$

Q can be derived by assuming there is a random, unknown acceleration in each coordinate that is constant over Δt, the interval between measurements, using Eqs. 4.9.47 and 4.9.50 from Tapley et al. [17]. A variance for the unknown acceleration, σ_i^2 is assumed for each spacecraft, with i representing the spacecraft number, and with x, y, and z components equal in magnitude. Assuming that Δt is small relative to the spacecraft orbital period, Q can be constructed as a 6×6 matrix for each spacecraft with the following form:

$$\begin{bmatrix} \frac{\Delta t^4}{3}\sigma_i^2 & 0 & 0 & \frac{\Delta t^3}{2}\sigma_i^2 & 0 & 0 \\ 0 & \frac{\Delta t^4}{3}\sigma_i^2 & 0 & 0 & \frac{\Delta t^3}{2}\sigma_i^2 & 0 \\ 0 & 0 & \frac{\Delta t^4}{3}\sigma_i^2 & 0 & 0 & \frac{\Delta t^3}{2}\sigma_i^2 \\ \frac{\Delta t^3}{2}\sigma_i^2 & 0 & 0 & \Delta t^2\sigma_i^2 & 0 & 0 \\ 0 & \frac{\Delta t^3}{2}\sigma_i^2 & 0 & 0 & \Delta t^2\sigma_i^2 & 0 \\ 0 & 0 & \frac{\Delta t^3}{2}\sigma_i^2 & 0 & 0 & \Delta t^2\sigma_i^2 \end{bmatrix} \tag{4}$$

The values of σ_i were tuned until they resulted in a realistic estimation error covariance matrix and low state errors. Usually the values of σ_i for the halo orbiters were different than for the lunar orbiters. State errors were computed by differencing the estimated state with the true state at each measurement time.

IV. Navigation Simulations

A. L_2 Halo-Low Lunar Orbiter

A navigation and communication relay mission to the moon was designed that would involve two spacecraft: one in a halo orbit at Earth–moon L_2 and another in a low lunar orbit (LLO) with a polar inclination [18]. The halo orbit at L_2 is roughly 90,000 km across its largest dimension and is inclined so that it remains above the south pole of the moon for 7.9 days out of its 13.6-day period. The lunar orbiter would carry sensors for lunar science and provide intermittent coverage for the lunar poles as well as other areas of the moon's surface. Both could be used as tracking stations for spacecraft orbiting, landing, or roving at the moon.

After generating truth orbits for both spacecraft, crosslink range observations were computed every 60 s, unless the moon blocked the line of sight, and normally distributed noise with a standard deviation of 1 m was applied. The measurements were used in the EKF to estimate the state vector, which consisted of three-dimensional position and velocity for each spacecraft and a range bias. Although the reflectance parameters for the spacecraft can be estimated quite well using this measurement type, they were fixed with random errors to simulate SRP modeling errors. The a priori state for the EKF was computed with random, uncorrelated, and normally distributed position, velocity, and reflectance errors. The initial positions had errors in each component of 1 km (1σ) for the halo orbiter and 100 m (1σ) for the lunar orbiter. The velocity errors in each component were 1 mm/s (1σ) for the halo orbiter and 4 mm/s (1σ) for the lunar orbiter. These a priori errors were chosen to be slightly larger than the steady-state errors. The a priori estimation error covariance matrix was diagonal with position and velocity standard deviations 10 times larger than the actual errors.

The state estimates from the EKF were used to initialize the SKM computations for both spacecraft. Because lunar mass concentrations and the Earth's gravity will cause a spacecraft in LLO to drift away from its orbit and eventually crash into the moon, SKMs for the LLO were designed to restore the perilune and apolune altitudes to 50 and 95 km, respectively. Because both types of SKMs had 5% errors in execution, the velocity variances of the estimation error covariance matrix were increased accordingly after each maneuver. In that way, the EKF could be used properly to estimate the thruster error after the maneuver. The SKMs for the halo orbiter were performed 4 times per halo orbit period as described earlier, and LLO SKMs were performed once per halo period, halfway between two of the halo SKMs.

Because the two spacecraft would need to perform communication relay duties as well as provide tracking support to user spacecraft, they would not be available to track each other all the time. A realistic schedule was created specifying when the two spacecraft could track each other, and when the two spacecraft would be performing other duties. As much as possible, the tracking periods in the schedule were adjusted so that they would occur when the moon did not block the line of sight between the two spacecraft. The tracking occurred 9 times per day in 1-h blocks, with outages lasting as long as 5 h.

Figures 1–4 show the resulting accuracy for a sample run of the EKF over two halo periods (≈27 days) starting on 5 March 2012. The halo orbit SKMs show up in Fig. 2 as large increases in velocity uncertainty that occur with a 3.4-day period, with the jumps in uncertainty decreasing in magnitude as the maneuvers become smaller due to improved stationkeeping and orbit estimates. The increased uncertainty following a maneuver was added because of the thruster modeling errors in the simulation. Because of the short orbital period of the LLO and the long time scale in the plots, the results for the LLO appear noisy in Figs. 3 and 4. The LLO SKMs appear in both plots as spikes in uncertainty around day 8 and day 23. RMS and rss values for the trajectory errors were computed after day 8, excluding 90-min periods after each LLO SKM to let the filter converge on a new solution.

The estimation errors (computed after day 8) for ten 27-day simulations give an average position error for the halo orbiter of 132 m rss and an average velocity error of 0.6 mm/s rss. For the

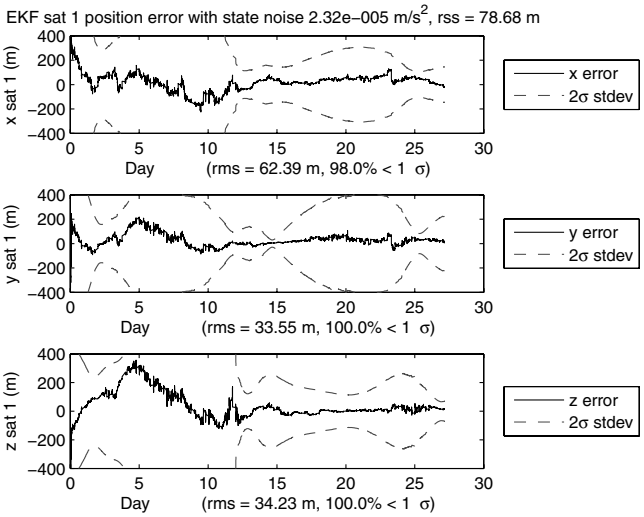

Fig. 1 Halo orbiter position accuracy using the EKF. Values for rms and rss were computed after day 8.

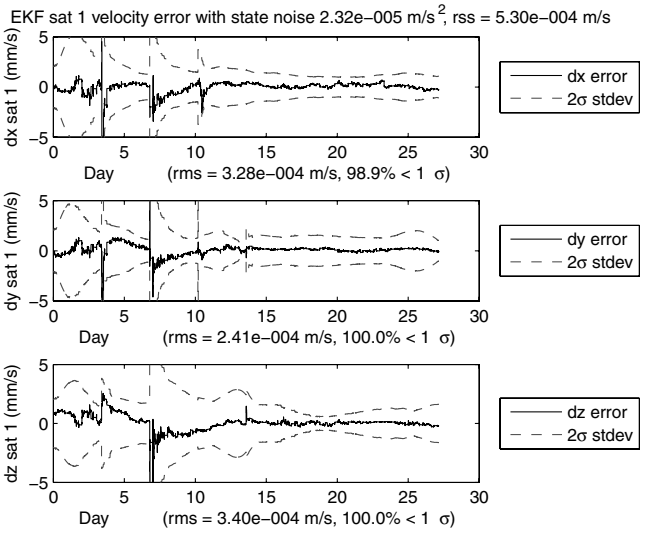

Fig. 2 Halo orbiter velocity accuracy using the EKF. Values for rms and rss were computed after day 8.

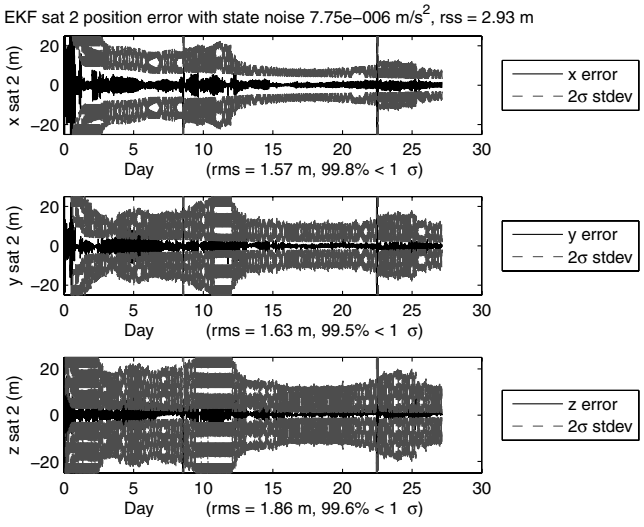

Fig. 3 Lunar orbiter position accuracy using the EKF. Values for rms and rss were computed after day 8.

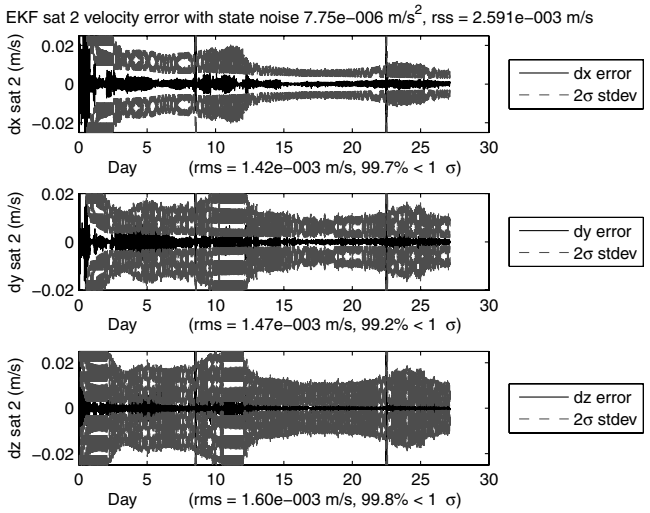

Fig. 4 Lunar orbiter velocity accuracy using the EKF. Values for rms and rss were computed after day 8.

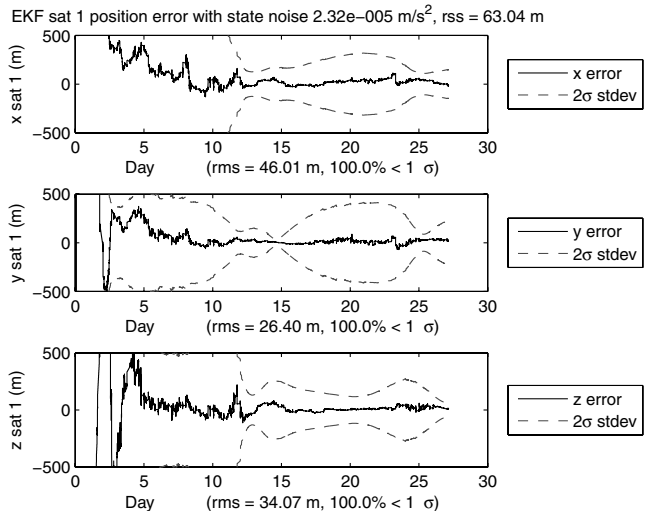

Fig. 5 Halo orbiter position accuracy using the EKF and large a priori errors. Values for rms and rss were computed after day 8.

lunar orbiter, the position error was 5.0 m rss and 4.4 mm/s rss for velocity, averaged over 10 runs. The range bias of 5 m was estimated to within several meters. The estimation error covariance for the LLO seems to reach a low steady-state value in about 2 days. Although more difficult to judge, it seems to take about 3–7 days for the halo orbit covariance to reach a low steady-state value. The average halo stationkeeping budget for the 10 runs was 2.0 m/s per year, excluding the numbers from the first two maneuvers in each run when the stationkeeping had not yet reached steady state. This is similar to other estimates of lunar halo stationkeeping budgets [19].

Next, the initial position and velocity errors and a priori standard deviations were increased by a factor of 10. The resulting initial positions had errors in each component of 10 km (1σ) for the halo orbiter and 1 km (1σ) for the lunar orbiter. The velocity errors were 1 cm/s (1σ) for the halo orbiter and 4 cm/s (1σ) for the lunar orbiter. Even with these large errors, the EKF still converges on the correct state estimate, as shown in Fig. 5. The estimate error covariance appears to be independent of the a priori covariance after about 9 days.

Table 1 Orbital elements for a three-satellite lunar communications constellation in frozen orbits

s/c no.	a, km	e	i^{op},[a] deg	Ω^{op},[a] deg	ω^{op}, deg	M^{op}, deg
1	6541.4000	0.6	56.2	0	90	0
2	6543.9759	0.6	56.2	0	90	120
3	6537.9213	0.6	56.2	0	90	240

[a] The superscript "op" means the frame is at the moon with the z axis parallel to the normal of the Earth's apparent orbit around the moon. These elements are for the epoch of 15 July 2009. Credit: Ely and Lieb [20].

B. NASA Lunar Frozen Orbiter Constellation

Ely and Lieb [20] show that three spacecraft in a lunar frozen orbit that lingers over the south pole of the moon can provide redundant communication coverage for surface missions there, while almost eliminating the cost of stationkeeping. These orbits are selected to "freeze" the argument of perilune and eccentricity to prevent collision with the lunar surface. Table 1 shows the orbital elements for lunar orbits that are frozen, or remain stable, even in the presence of SRP perturbations.

Although liaison navigation was shown to work well for halo orbiters in the vicinity of L_1 and L_2, it was not known if the third-body perturbation of the Earth would enable autonomous orbit determination if all the participating spacecraft were in lunar frozen orbits. The third-body perturbation of the Earth on a lunar orbiter is much stronger than the lunar perturbation on an Earth orbiter. These frozen orbits have a high altitude (about 8000 km) above the moon at apolune, so the Earth's third-body perturbation is quite significant.

Truth orbits similar to frozen orbits were propagated for three spacecraft using the orbital elements shown in Table 1. Using the truth orbits, crosslink range measurements were generated every 5 min when the moon did not block the line of sight. These crosslink range measurements were only generated for one pair of satellites at a time, in 1-h blocks. Then Gaussian noise with a standard deviation of 1 m was added to the measurements. The same modeling errors mentioned in Sec. IV.A were used in the EKF again. The orbits and EKF simulation extended over a 24-day span. Even after optimizing the state noise parameters and trying different initial state errors, the orbit estimates always converged on the wrong solution due to problems with observability, as shown in Fig. 6 for satellite 1.

Because these three spacecraft are in the same orbital plane, the out-of-plane component is not well resolved [3]. To eliminate this problem, Ω_2^{op} and Ω_3^{op} were set to 120 and 240 deg, respectively, so the three satellites would be in different orbital planes. The results were better, as shown for satellite 1 in Fig. 7, but still the estimates did not converge properly over time. The absolute orientation was unobservable in this case, meaning that the Earth's gravitational perturbation was not sufficiently strong to enable liaison navigation for this constellation.

C. Hybrid L_2/Frozen Orbit Constellation

Because both L_2 halo orbits and frozen orbits have distinct advantages, a hybrid constellation consisting of a halo orbiter and a spacecraft in a lunar frozen orbit could provide the benefits of both. The halo orbiter was placed in a quasi-halo orbit at L_2, and the lunar orbiter was placed in a frozen orbit with the orbital elements from Table 1. The two spacecraft tracked each other and a crosslink range measurement was generated every 5 min. The a priori state for the EKF was computed with random, uncorrelated, and normally distributed position, velocity, and reflectance errors. The initial positions had errors in each component of 1 km (1σ) for the halo orbiter and 100 m (1σ) for the lunar orbiter. The velocity errors were 1 mm/s (1σ) for the halo orbiter and 4 mm/s (1σ) for the lunar orbiter. The state noise parameters were tuned as before. SKMs were not necessary for the frozen orbit, but were performed in the same manner as before for the halo orbiter. The results for position estimation are shown in Fig. 8 for the halo orbiter and Fig. 9 for the lunar orbiter over two halo periods starting on 5 March 2012. The estimation errors (computed after day 8) for ten 27-day simulations give an average position error for the halo orbiter of 87 m rss and an average velocity error of 0.4 mm/s rss. For the lunar orbiter, the position error was 9.8 m rss and 1.4 mm/s rss for velocity. The average stationkeeping budget for the 10 runs was 2.6 m/s per year.

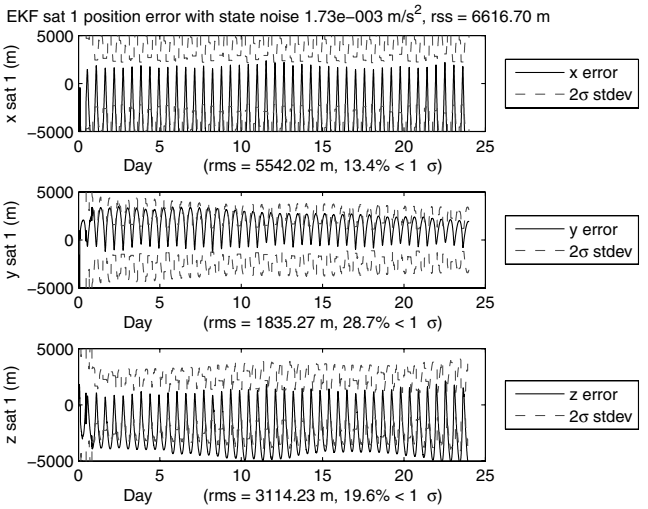

Fig. 6 Satellite 1 position accuracy using the EKF. The three satellites are in coplanar orbits similar to frozen orbits. Values for rms and rss were computed after day 8.

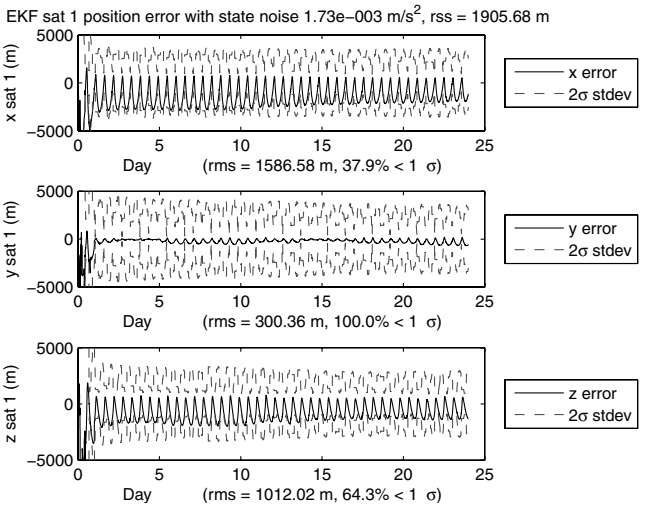

Fig. 7 Satellite 1 position accuracy using the EKF. The three satellites are in orbits similar to lunar frozen orbits in three different orbit planes. Values for rms and rss were computed after day 8.

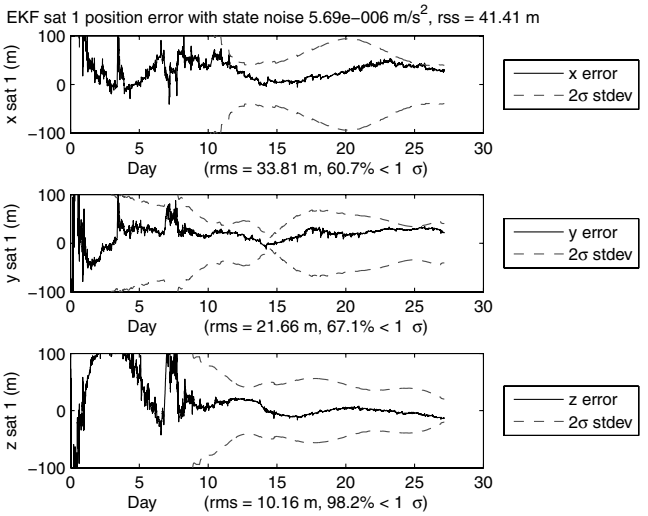

Fig. 8 L_2 halo orbiter EKF position accuracy using crosslink range measurements to a lunar spacecraft in a frozen orbit. Values for rms and rss were computed after day 8.

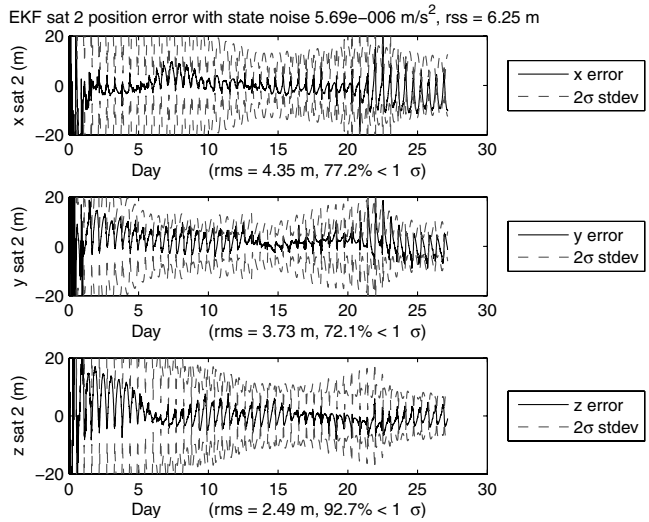

Fig. 9 Lunar pole-lingering frozen orbit EKF position accuracy using crosslink range measurements to a halo orbiter at L_2. Values for rms and rss were computed after day 8.

When computing the stationkeeping budget, the first two maneuvers in each run were ignored because they were performed before the spacecraft had reached a steady-state stationkeeping error.

D. L_1/LEO Constellation

In case no lunar orbiters were available for tracking from a halo orbit, a final simulation was performed to investigate the feasibility of using an Earth orbiter instead. For this simulation, the Earth was the center of the coordinate system, and a spacecraft was placed in a circular low Earth orbit (LEO) at 800-km altitude and 60 deg inclination. Another spacecraft was placed in a lunar L_1 halo orbit. The JGM-3 gravity field [10] was used for the truth orbits to degree and order 50. A $1-\sigma$ clone of the JGM-3 gravity field was provided by John Ries of the Center for Space Research at the University of Texas, and used in the EKF to simulate gravity modeling errors.

Crosslink range measurements were generated every 6 min, with all other parameters set up similar to the other simulations. Over 10 runs, the average rss position errors are 512 and 11 m for the halo orbiter and LEO orbiter, respectively. Even though these results are good, they are not as accurate as the L_2/frozen orbit constellation described in Sec. IV.C. This is probably because from L_1 to Earth, the long link distance means that crosslinks are generally in the same direction. However, from L_2 to a frozen orbit, the crosslinks are more geometrically diverse as the halo orbiter goes around its orbit. Also, the tracking data in the L_1/LEO case provided too little information to estimate the range bias properly.

V. Conclusions

This study showed that liaison navigation will work for a constellation of spacecraft, as long as one is in a libration point orbit such as a halo orbit. Realistic simulations showed that liaison navigation can be used to obtain excellent autonomous orbit estimates with position accuracies on the order of 100 m rss for lunar libration point orbiters, and 10 m rss for lunar orbiters. In these simulations, lunar halo orbiters using liaison navigation and the Genesis stationkeeping strategy had stationkeeping ΔV budgets as small as 2 m/s per year. Lunar halo orbiters can provide communication relay services for future lunar missions to the far side or the poles of the moon and liaison navigation would reduce the amount of Earth-based tracking required to maintain the constellation. A constellation with spacecraft in both halo orbits and lunar frozen orbits is ideal for autonomous orbit determination, results in small stationkeeping budgets, and would provide excellent communication coverage.

Acknowledgment

This material is based upon work supported under a National Science Foundation Graduate Research Fellowship.

References

[1] Thornton, C. L., and Border, J. S., *Radiometric Tracking Techniques for Deep-Space Navigation*, Monograph 1, Deep-Space Communications and Navigation Series, Jet Propulsion Laboratory, California Institute of Technology, Pasadena, CA, 2000.

[2] Markley, F. L., "Autonomous Navigation Using Landmark and Intersatellite Data," AIAA Paper 1984-1987, Aug. 1984.

[3] Hill, K., and Born, G., "Autonomous Interplanetary Orbit Determination Using Satellite-to-Satellite Tracking," *Journal of Guidance, Control, and Dynamics*, Vol. 30, No. 3, 2007, pp. 679–686. doi:10.2514/1.24574

[4] Psiaki, M. L., "Autonomous Orbit Determination for Two Spacecraft from Relative Position Measurements," *Journal of Guidance, Control, and Dynamics*, Vol. 22, No. 2, 1999, pp. 305–312.

[5] Hill, K., *TurboProp Ver. 3.2 User's Manual*, Colorado Center For Astrodynamics Research, 2007, http://ccar.colorado.edu/geryon/papers/TurboProp 3 2 Manual.pdf.

[6] Standish, E. M., Newhall, X. X., Williams, J. G., and Folkner, W. M., "JPL Planetary and Lunar Ephemerides, DE403/LE403," Jet Propulsion Laboratory IOM 314.10-127, 22 May 1995.

[7] Ma, C., Arias, E., Eubanks, T., Fey, A., Gontier, A., Jacobs, C., Sovers, O., Archinal, B., and Charlot, P., "The International Celestial Reference Frame as Realized by Very Long Baseline Interferometry," *Astronomical Journal*, Vol. 116, No. 1, 1998, pp. 516–546. doi:10.1086/300408

[8] Hoffman, D., "A Set of C Utility Programs for Processing JPL Ephemeris Data," NASA Johnson Space Center, ftp://ssd.jpl.nasa.gov/pub/eph/export/C-versions/hoffman, 3 August 1998.

[9] Konopliv, A., Asmar, S. W., Carranza, E., Sjogren, W. L., and Yuan, D., "Recent Gravity Models as a Result of the Lunar Prospector Mission," *Icarus*, Vol. 150, No. 1, 2001, pp. 1–18. doi:10.1006/icar.2000.6573

[10] Tapley, B., Watkins, M., Ries, J., Davis, G., Eanes, R., Poole, S., Rim, H., Schutz, B., Shum, C., Nerem, R., Lerch, F., Marshall, J., Klosko, S., Pavlis, N., and Williamson, R., "The Joint Gravity Model 3," *Journal of Geophysical Research*, Vol. 101, No. B12, 1996, pp. 28029–28050. doi:10.1029/96JB01645

[11] Newhall, X. X., and Williams, J. G., "Estimation of the Lunar Physical Librations," *Celestial Mechanics and Dynamical Astronomy*, Vol. 66, No. 1, 1997, pp. 21–30. doi:10.1007/BF00048820

[12] Vallado, D., and McClain, W., *Fundamentals of Astrodynamics and Applications*, 3rd ed., Microcosm Press, El Segundo, CA, 2007.

[13] Farquhar, R. W., "The Control and Use of Libration-Point Satellites," NASA TR R-346, 1970.

[14] Howell, K., "Three-Dimensional, Periodic, 'Halo' Orbits," *Celestial Mechanics and Dynamical Astronomy*, Vol. 32, No. 1, 1984, pp. 53–71.

[15] Howell, K., and Pernicka, H., "Numerical Determination of Lissajous Trajectories in the Restricted Three-body Problem," *Celestial Mechanics*, Vol. 41, Nos. 1–4, March 1987, pp. 107–124. doi:10.1007/BF01238756

[16] Williams, K., Wilson, R., Lo, M., Howell, K., and Barden, B., "Genesis Halo Orbit Station Keeping Design," *International Symposium: Spaceflight Dynamics*, CNES, Paris, 26 June 2000.

[17] Tapley, B. D., Schutz, B. E., and Born, G. H., *Statistical Orbit Determination*, Elsevier Academic Press, Burlington, MA, 2004.

[18] Hill, K., Parker, J., Born, G. H., and Demandante, N., "A Lunar L_2 Navigation, Communication, and Gravity Mission," AIAA Paper 2006-6662, Aug. 2006.

[19] Gómez, G., Howell, K., Masdemont, J., and Simó, C., "Station-Keeping Strategies for Translunar Libration Point Orbits," *Spaceflight Mechanics 1998*, Advances in the Astronautical Sciences, Vol. 98, Univelt, San Diego, CA, 1998, pp. 949–958.

[20] Ely, T. A., and Lieb, E., "Constellations of Elliptical Inclined Lunar Orbits Providing Polar and Global Coverage," *Journal of the Astronautical Sciences*, Vol. 54, No. 1, 2006, pp. 53–67.

C. McLaughlin
Associate Editor